ISSN 0021-3640, JETP Letters, 2019, Vol. 109, No. 4, pp. 276–279. © Pleiades Publishing, Inc., 2019.
Russian Text © The Author(s), 2019, published in Pis'ma v Zhurnal Eksperimental'noi i Teoreticheskoi Fiziki, 2019, Vol. 109, No. 4, pp. 265–268.

CONDENSED MATTER

Proximity of Ferromagnetic Nickel to Paramagnetic Instability

N. G. Zamkova[a], *, V. A. Gavrichkov[a], **, I. S. Sandalov[a], and S. G. Ovchinnikov[a], ***

[a] *Kirensky Institute of Physics, Federal Research Center KSC, Siberian Branch, Russian Academy of Sciences, Krasnoyarsk, 660036 Russia*

**e-mail: zam@iph.krasn.ru*

***e-mail: gav@iph.krasn.ru*

****e-mail: sgo@iph.krasn.ru*

Received December 17, 2018; revised December 17, 2018; accepted December 18, 2018

The phase diagram of Ni in the space of the parameters has been studied within the Kanamori model with the parameters determined from comparison with ab initio calculations for ferromagnetic Ni. The proximity of Ni to the boundary of the transition to a paramagnetic state has been found.

DOI: 10.1134/S0021364019040131

1. Recent experiments on femtosecond magnetooptics revealed possibilities of ultrafast optical control of the magnetic order [1]. Most of the experiments on ultrafast demagnetization in metallic magnets were performed with ferromagnetic Ni films, where this phenomenon was detected for the first time [2], and in the GdFe ferromagnet [3]. The mechanisms of ultrafast demagnetization in metals are still unclear. Analysis of many published works shows that the main attention is focused on the extension of ab initio calculations to different variants of the Heisenberg model [4–6]. According to our studies of the role of the local environment in the formation of the magnetic moment [7, 8], such an approach fundamentally cannot describe one of the most important competing mechanisms. Namely, since electrons describing localized spins in the Heisenberg model are always localized, they cannot be involved in the formation of delocalized electron bands and cannot make an additional contribution to the binding energy of the crystal (one of the brightest examples is a gamma–alpha transition in cerium, where the delocalization of one f electron leads to the 15% contraction of the lattice [9, 10]). We believe that the description of the relaxation (nonequilibrium dynamics) of a metal magnet excited by a femtosecond laser pulse requires the solution of three problems: (i) the description of the initial thermodynamic state and its temperature evolution at the initial time instant, (ii) the study of the contribution of the initial correlations, and (iii) relaxation from the nonequilibrium state. In this work, we solve the first problem for nickel. Ab initio methods based on the density functional theory make it possible to calculate the electronic structure of nickel and to show that the ferromagnetic state is lower in energy than the paramagnetic one. Temperature dependences of the magnetization and susceptibility at high temperatures are calculated [11–14] with the inclusion of the Anderson impurity model (LDA + DMFT). The model thus obtained implicitly includes open problems such as the double counting of the Coulomb interaction between d electrons and the applicability of the impurity approach to a regular crystal. These problems complicate the understanding of the physics of formation of the mechanism. An alternative approach is based on the study of the phase diagram of possible states in the space of the parameters of the multielectron model Hamiltonian including symmetry and the numbers of orbitals and electrons of matter.

2. Here, to determine the region of stability of the ferromagnetic state of nickel on the phase diagram of states, we use a complex approach [7, 8] combining the ab initio calculation and the subsequent model analysis. The ab initio calculation of the electronic structure of Ni was performed with the VASP package in the generalized gradient approximation (GGA) [15, 16] using projector augmented wave (PAW) pseudopotentials [17, 18]. The exchange correlation potential was used with the Perdew–Burke–Ernzerhoff (PBE) parameterization [19, 20]. The cutoff energy of plane waves was 500 eV. Integration over the first Brillouin zone was performed using a $10 \times 10 \times 10$ Monkhorst–Pack grid [21]. The configuration of valence electrons of nickel was $3d^8 4s^2$. Metallic Ni has a face-centered cubic lattice ($a = 3.5$ Å) and is a ferromagnet ($\mu_{Ni} = 0.605\mu_B$, $T_c = 631$ K). The calculated lattice parameter of 3.51 Å and magnetic moment of $0.73\mu_B$ on a nickel atom are in good agreement with known experimental data.

Further, the results of the ab initio calculation are extended to the multiband Kanamori model [7, 8].

The model Hamiltonian includes intra-atomic Coulomb and exchange interactions (U, U', and J) and hopping integrals $t_{\lambda\mu}$ (subscripts λ and μ specify s, p, and d orbitals) between neighboring nickel atoms in the first coordination sphere:

$$H = H^{\mathrm{Ni}} + H_{\mathrm{hop}}, \quad H^{\mathrm{Ni}} = H_0^{\mathrm{Ni}} + H_{\mathrm{C}}^{\mathrm{Ni}}. \qquad (1)$$

Here,

$$H_{\mathrm{hop}} = \sum t_{\lambda\mu}^{nn'} c_{n\lambda\sigma}^{\dagger} c_{n'\mu\sigma} + \mathrm{H.c.};$$

$$H_0^{\mathrm{Ni}} = \sum (\varepsilon_0^s \hat{n}_{n\sigma}^s + \varepsilon_0^p \hat{n}_{nm\sigma}^p + \varepsilon_0^d \hat{n}_{nm\sigma}^d);$$

and the Coulomb part of the Hamiltonian has the form

$$H_{\mathrm{C}}^{\mathrm{Ni}} = \frac{U}{2} \sum \hat{n}_{nm\sigma}^d \hat{n}_{nm\bar{\sigma}}^d$$

$$+ \left(U' - \frac{1}{2} J\right) \sum \hat{n}_{nm}^d \hat{n}_{nm'}^d (1 - \delta_{mm'}) - \frac{1}{2} J \sum \hat{s}_{nm}^d \hat{s}_{nm'}^d,$$

where

$$\hat{n}_{nm\sigma}^d \equiv d_{nm\sigma}^{\dagger} d_{nm\sigma}, \quad \hat{n}_{nm}^d = \hat{n}_{nm\uparrow}^d + \hat{n}_{nm\downarrow}^d,$$

$$\hat{s}_{nm}^d \equiv \sigma_{\alpha\gamma} d_{nm\alpha}^{\dagger} d_{nm\gamma}, \quad \hat{n}_{nm\sigma}^p \equiv p_{nm\sigma}^{\dagger} p_{nm\sigma},$$

$$\hat{n}_{n\sigma}^s \equiv s_{n\sigma}^{\dagger} s_{n\sigma},$$

subscripts n and n' specify sites; λ, μ, m, and m' specify an orbital; σ is the spin index; and $\sigma_{\alpha\gamma}$ is the Pauli matrix. The wave vector dependence of hopping integrals is specified in the Slater–Koster scheme [22]. The eigenvalues of the model Hamiltonian are determined by the Green's function method in the Hartree–Fock approximation. The occupation numbers of all orbitals are determined self-consistently. All interaction constants are the model parameters determined from the condition that the model should reproduce the occupation numbers, magnetic moment on nickel atom, electron density of states, and band structure of this compound ab initio calculated with the VASP package. The model parameters were sought by the annealing method. The parameters providing the best fitting of model occupation numbers of orbitals and d electron density of states to ab initio calculations are summarized in Table 1.

Table 1. Model parameters (in electronvolts) ensuring the best approximation

U	J	U'	ε_s	ε_p	ε_{t2g}	ε_{e2g}
2.74	0.45	1.20	–4.37	14.84	–6.06	–6.61
Hopping integrals	t_{dd}	t_{dp}	t_{pp}	t_{ds}	t_{ps}	t_{ss}
σ	–0.28	–1.78	1.43	–1.52	1.12	–0.57
π	0.21	–0.73	0.7	–	–	–
δ	–0.16	–	–	–	–	–

Table 2. Model and ab initio (VASP) occupation numbers of the d orbitals ($n_{\uparrow}^d, n_{\downarrow}^d$), magnetic moment, and number of d electrons N_{el}

Orbital	VASP				Model			
	$n_{\uparrow}^d$	$n_{\downarrow}^d$	μ, μ_{B}	N_{el}	$n_{\uparrow}^d$	$n_{\downarrow}^d$	μ, μ_{B}	N_{el}
t_{2g}	0.90	0.70	0.73	8.2	0.85	0.65	0.74	8.0
e_g	0.91	0.81			0.90	0.84		

The results of the model calculations are presented in Table 2 and Fig. 1 in comparison with the parameters from Table 1 and the VASP calculations.

Analysis of the model makes it possible to explicitly reveal the role of different interactions in the forma-

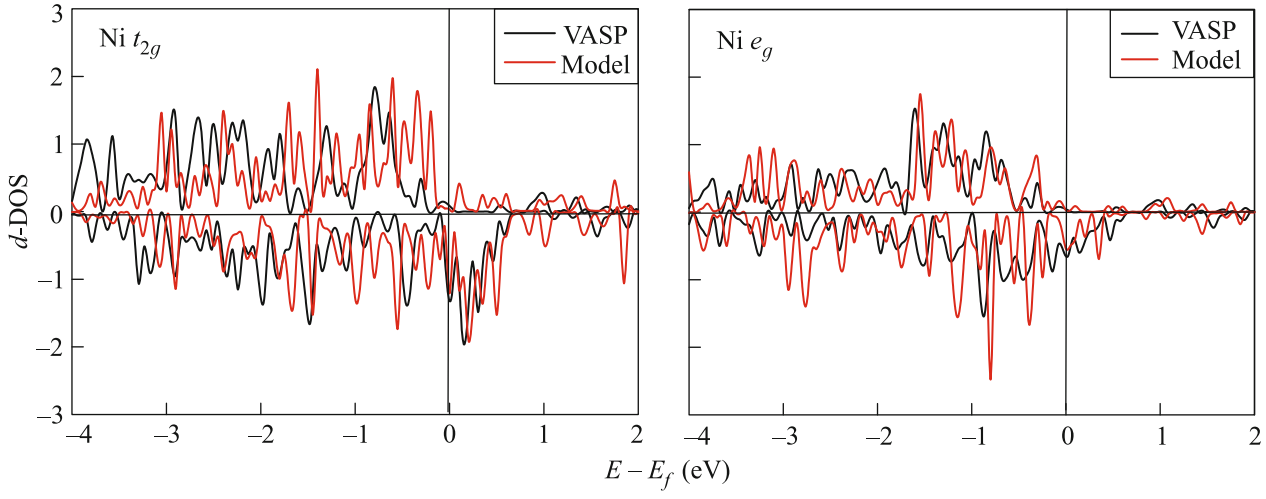

Fig. 1. (Color online) Ab initio and model d electron densities of states of nickel.

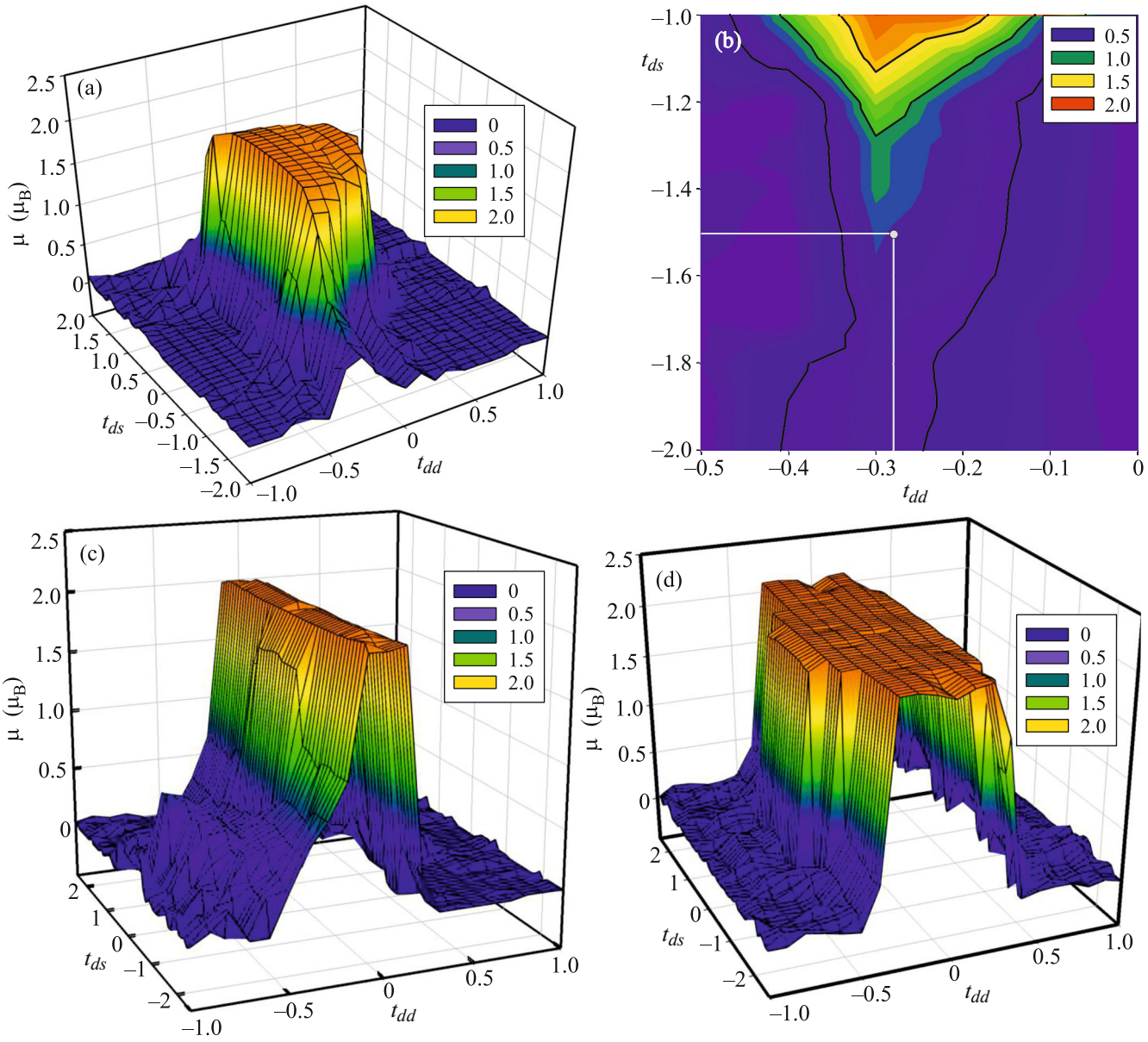

Fig. 2. (Color online) (a) Magnetic moment of the nickel atom versus the hopping integrals $t_{dd}^{\sigma}(\equiv t_{dd})$ and t_{ds}. (b) Region of the parameters near the values from Table 1. (c) Magnetic moment of the nickel atom versus the hopping integrals $t_{dd}^{\sigma}(\equiv t_{dd})$ and $t_{dp}^{\sigma}(\equiv t_{dp})$. (d) Magnetic moment of the nickel atom versus the hopping integrals $t_{dd}^{\sigma}(\equiv t_{dd})$ and $t_{dp}^{\sigma}(\equiv t_{dp})$ at $t_{ds} = 0$.

tion of the magnetic state in nickel and to determine the critical parameters. Two hopping integrals between d electrons (t_{dd}) and d and s electrons (t_{ds}) of neighboring atoms are two critical parameters for the appearance of ferromagnetism in nickel. The region of stability of the ferromagnetic state of nickel is shown in Fig. 2a, depending on the critical parameters t_{dd} and t_{ds}. When plotting maps of magnetic moments, all other hopping parameters are varied proportionally to the parameter t_{dd}^{σ}.

The dependence of the magnetic moment of nickel on both hopping parameters t_{dd} and t_{ds} is very sharp, and the experimentally observed magnetic moment (~$0.7\mu_B$) on the nickel atom is in a narrow interface between the ferro- and paramagnetic phases (Fig. 2b). The effect of other model parameters on the region of existence of the ferromagnetic phase is insignificant. In particular, Figs. 2c and 2d show maps of magnetic moments depending on the hopping integral t_{dp} between d and p electrons. As seen, the magnetic moment hardly depends on this parameter, whereas

the exclusion of the parameter t_{ds} results in the extension of the region of stability of the ferromagnetic phase. It is noteworthy that a sharp dependence of the magnetic moment on the parameter t_{dd} is characteristic not only for nickel but also for iron and manganese silicides [7, 8]. It can be expected that this feature of the model phase diagrams will hold for other compounds with 3*d* transition metals. However, if the magnetic moment on a transition metal atom is large (e.g., $\mu \sim 2.0\mu_B$ as in bcc-Fe), the experimentally observed ferromagnetic state will occur in a more stable part of the phase diagram rather than in the region of instability, i.e., near the sharp interface between the ferro- and paramagnetic phases.

3. Our conclusion on the proximity of ferromagnetic Ni to paramagnetic instability has been obtained for an equilibrium state. Obviously, this conclusion cannot directly explain the reasons for ultrafast demagnetization. However, since ultrafast demagnetization in the GdFe ferromagnet is also observed at temperatures near the point of compensation of two sublattices [14], i.e., near instability of the magnetic structure, it can be hypothesized that the proximity of the system to magnetic instability is a determining factor for ultrafast demagnetization irrespective of particular microscopic mechanisms. The determination of microscopic ultrafast demagnetization mechanisms is certainly an actual unsolved problem of magnetism.

This work was supported by the Russian Foundation for Basic Research (project no. 16-02-00273).

REFERENCES

1. A. Kirilyuk, A. V. Kimel, and T. Rasing, Rev. Mod. Phys. **82**, 2732 (2010).
2. E. Beaurepaire, J.-C. Merle, A. Daunois, and J.-Y. Bigot, Phys. Rev. Lett. **76**, 4250 (1996).
3. I. Radu, K. Vahaplar, C. Stamm, T. Kachel, N. Pontius, H. A. Dürr, T. A. Ostler, J. Barker, R. F. L. Evans, R. W. Chantrell, A. Tsukamoto, A. Itoh, A. Kirilyuk, Th. Rasing, and A. V. Kimel, Nature (London, U.K.) **472**, 205 (2011).
4. F. Körmann, A. Dick, T. Hickel, and J. Neugebauer, Phys. Rev. B **83**, 165114 (2011).
5. A. Dick, F. Körmann, T. Hickel, and J. Neugebauer, Phys. Rev. B **84**, 125101 (2011).
6. F. Körmann, B. Grabowski, B. Dutta, T. Hickel, L. Mauger, B. Fultz, and J. Neugebauer, Phys. Rev. Lett. **113**, 165503 (2014).
7. V. S. Zhandun, N. G. Zamkova, S. G. Ovchinnikov, and I. S. Sandalov, Phys. Rev. B **95**, 054429 (2017).
8. N. G. Zamkova, V. S. Zhandun, S. G. Ovchinnikov, and I. S. Sandalov, J. Alloys Compd. **695**, 1213 (2017).
9. D. G. Koskenmaki and K. A. Gschneidner, Jr., *Handbook on the Physics and Chemistry of Rare Earths* (Elsevier, New York, 1979), Vol. 1, p. 337.
10. M. J. Lipp, D. Jackson, H. Cynn, C. Aracne, W. J. Evans, and A. K. McMahan, Phys. Rev. Lett. **101**, 165703 (2008).
11. A. I. Lichtenstein, M. I. Katsnelson, and G. Kotliar, Phys. Rev. Lett. **87**, 067205 (2001).
12. I. A. Nekrasov, N. S. Pavlov, and M. V. Sadovskii, JETP Lett. **95**, 581 (2012).
13. J. Sweep, A. N. Rubtsov, and M. I. Katsnelson, JETP Lett. **98**, 427 (2013).
14. M. A. Korotin, N. A. Skorikov, S. L. Skornyakov, A. O. Shorikov, and V. I. Anisimov, JETP Lett. **100**, 823 (2014).
15. G. Kresse and J. Furthmuller, Comput. Mat. Sci. **6**, 15 (1996).
16. G. Kresse and J. Furthmuller, Phys. Rev. B **54**, 11169 (1996).
17. P. E. Blochl, Phys. Rev. B **50**, 17953 (1994).
18. G. Kresse and D. Joubert, Phys. Rev. B **59**, 1758 (1999).
19. J. P. Perdew, K. Burke, and M. Ernzerhof, Phys. Rev. Lett. **77**, 3865 (1996).
20. J. P. Perdew, K. Burke, and M. Ernzerhof, Phys. Rev. Lett. **78**, 1396 (1997).
21. H. J. Monkhorst and J. D. Pack, Phys. Rev. B **13**, 5188 (1976).
22. J. C. Slater and G. F. Koster, Phys. Rev. **94**, 1498 (1954).

Translated by R. Tyapaev